Applied Catalysis B: Environmental 184 (2016) 223–237

Contents lists available at ScienceDirect

Applied Catalysis B: Environmental

journal homepage: www.elsevier.com/locate/apcatb

The ILs-assisted solvothermal synthesis of TiO_2 spheres: The effect of ionic liquids on morphology and photoactivity of TiO_2

Marta Paszkiewicz[a], Justyna Łuczak[b,*], Wojciech Lisowski[c], Paulina Patyk[a], Adriana Zaleska-Medynska[a,b,*]

[a] Department of Environmental Technology, Faculty of Chemistry, University of Gdansk, Wita Stwosza 63, 80-308 Gdansk, Poland
[b] Department of Chemical Technology, Faculty of Chemistry, Gdansk University of Technology, G. Narutowicza 11/12, 80-233 Gdansk, Poland
[c] Mazovia Center for Surface Analysis, Institute of Physical Chemistry, Polish Academy of Science,. Kasprzaka 44/52, 01-244 Warszawa, Poland

ARTICLE INFO

Article history:
Received 26 August 2015
Received in revised form 26 October 2015
Accepted 16 November 2015
Available online 1 December 2015

Keywords:
Ionic liquids
ILs-assisted synthesis
TiO_2 microspheres
TiO_2 particles
Heterogeneous photocatalysis
Solvothermal synthesis

ABSTRACT

Effect of the ionic liquid (IL) structure (chain length in the imidazolium cation) on morphology and photoactivity of TiO_2 particles has been systematically investigated. The TiO_2 microspheres have been successfully synthesized via facile solvothermal method assisted by ionic liquids, such as 1-butyl-3-methylimidazolium chloride [BMIM][Cl] and 1-decyl-3-methylimidazolium chloride [DMIM][Cl] using tetra-tert-butyl orthotitanate (TBOT) as a TiO_2 precursor. Surface properties were characterized using scanning electron microscopy (SEM), transmission electron microscopy (TEM), X-ray powder diffraction analysis (XRD), BET surface area measurement, elemental analysis (NCHS) and X-ray photoelectron spectroscopy (XPS). The photocatalytic activity was investigated by means of phenol photodegradation in the aqueous phase as a model pollutant, as well as formation of hydroxyl radicals based on detection of fluorescent product of coumarine hydroxylation. Surface properties of TiO_2 particles were correlated with the type and amount of the IL used during preparation as well as with the photoactivity. Both mechanism of the TiO_2 spheres formation in the presence of [BMIM][Cl] and [DMIM][Cl] likewise the mechanism of their photoexcitation were also discussed. It was found that both electrostatic stabilization as well as coordination by imidazolium cation was responsible for securing the growth of the TiO_2 spheres. The XPS data clearly revealed that the amount of carbon in the form of N—C=N species (imidazole-metal bound formed through C-2 carbon in imidazole ring) corresponds well with the change of the photoactivity. The most active samples (phenol degradation rate: 5.9 $mmol \cdot dm^{-3} \cdot min^{-1}$) contained the highest amount of carbon in the form of N—C=N species (6.06 at.%) among all ILs-TiO_2 samples.

1. Introduction

Photocatalytic reactions at the surface of titanium dioxide (TiO_2) have been attracting much attention in view of their practical applications to environmental cleaning such as self-cleaning surfaces, water, wastewater and air treatment, bacteria inactivation and hydrogen generation via water splitting [1–4]. The photocatalytic activity of TiO_2 can be controlled by proper of the preparation route, and as a consequence by controlling some physical and structural properties of the photocatalysts, i.e., specific surface area, density and crystalline defects, primary and secondary particle size, existence of anatase and rutile phases, particles shape [5–7]. TiO_2 particles in the form of mesoporous precipitate, as well as oriented structures such as nanotubes, nanorods, nano- and microspheres, hollow microspheres or flower-like structures could be obtained by sol–gel, hydrothermal, solvothermal, sonochemical or chemical vapor deposition methods [8].

Recently, ionic liquids (ILs) have received a great interest in the synthesis of the nano- and microparticles [9,10] due to their superior properties such as low vapor pressure, melting point below 100 °C, high polarity as well as good thermal, dissolving and transport properties [11–13]. The real strength of the ionic liquids is related with the possibility to modify the cation and anion structure (ILs are frequently termed “designer solvents”), and as a consequence to alter their physicochemical properties, hence possible interactions with colloidal particle. Therefore, the interplay between Coulomb, van der Waals, π - π interactions and hydrogen bonding makes ILs potential key tool in the preparation of a new generation of nano- and microstructures [14]. Due

* Corresponding authors.
E-mail addresses: justyna.luczak@pg.gda.pl (J. Łuczak), adriana.zaleska@ug.edu.pl (A. Zaleska-Medynska).

http://dx.doi.org/10.1016/j.apcatb.2015.11.019
0926-3373/

Table 1
Sample label, applied ions, molar ratio of reagents (IL:TBOT), surface properties and photoactivity of IL-assisted TiO_2.

Sample label	Cation of IL	Anion of IL	Molar ratio (IL:TBOT)	Crystalline size (nm)	S_{BET} ($m^2\,g^{-1}$)	Pore volume ($cm^3\,g^{-1}$)	Phenol degradation reaction rate ($mmol\,dm^{-3}\,min^{-1}$)
TiO_2	–	–	–	6.6	184	0.069	5.2
TiO_2_B(1:10)	[BMIM]	[Cl]	1:10	7.2	196	0.058	5.3
TiO_2_B(1:2)	[BMIM]	[Cl]	1:2	7.2	202	0.059	5.9
TiO_2_B(1:1)	[BMIM]	[Cl]	1:1	10.1	201	0.098	3.2
TiO_2_D(1:10)	[DMIM]	[Cl]	1:10	8.4	203	0.059	5.1
TiO_2_D(1:2)	[DMIM]	[Cl]	1:2	8.4	218	0.065	5.5
TiO_2_D(1:1)	[DMIM]	[Cl]	1:1	9.7	188	0.092	3.7

to the intrinsic charge, ILs can create an electrostatic stabilization of the colloidal particles [15,16], alkyl substituent in the cation may provide steric hindrance [17], whereas amphiphilic structure of ILs [18] determine their ability to form protective electrosteric shell around the colloidal particle. Additional stabilization may also come from ILs viscosity, since aggregation rate of particles in ionic liquids appears to become lower than that in water or classical organic solvents. Higher viscosity of the ILs decreases Brownian motions, hence mass transfer of solute and finally agglomeration [9,19]. These interactions can be enriched in the coordination ability of both cation and/or anion (especially functionalized) [16,20]. Moreover, ILs may constitute a source of fluoride anions generated in situ required for the nanoparticles precipitation [21], self-assemble into organized structures in aqueous/nonaqueous solutions [22,23], support micelle formation by conventional surfactants [24] or form microemulsion systems [25,26]. In this regard ionic liquids may play a role of a solvent, soft template, reagent, agent promoting reduction of the precursor or particles stabilizer during synthesis of inorganic materials [9,20,27].

Up to date, most of the research involving the IL supported nano- and microparticles synthesis were focused on the monometallic structures formation (Ru, Rh, Pd, Ag, Au, Ir, and some others) [28]. The relative size and the morphology of the particles can be adjusted, since it was found that the size of the metal particles is directly related to the length of the alkyl imidazolium side chain as well as the IL's anion volume and coordination ability. Neutral metal precursors tend to be dissolved in the IL nonpolar domains [29,30], and therefore, the size of the nanoparticles increases with the elongation of the alkyl side chain in the imidazolium cation. However, the relative size of the metal nanoparticles prepared based on the ionic precursors are related to the volume of the polar nanoregions since the ionic precursors are located in the polar nanodomains of ILs [30]. For that reason, the average diameter of the particles prepared from ionic precursors may exhibit opposite relation. In addition, the relative size of the metal NPs can be also related to the coordination ability of the IL anion. By using as reaction media ILs composed of a more coordinated anion smaller nanoparticles can be obtained [31,32].

Much less attention was devoted to semiconductors, therefore, we intend to take into account TiO_2 semiconductor prepared in the IL assisted solvothermal way. Up to date, hydro- and solvothermal syntheses using ILs were applied to formation of the CuO, ZnSe, MoS_2, NiO, BiOBr, MnO, CdS, and CdSe among others [33–40]. It was revealed that selection of ionic liquid allows to achieve the desired physical and structural properties of the particles. Much less investigations was devoted to IL/TiO_2 systems. Jing et al. [41] synthesized TiO_2 modified by 1-allyl-3-(butyl-4-sulfonyl) imidazolium hydrosulfate [ABsIM][HSO_4] by hydrothermal method, resulting in covalently functionalized IL-TiO_2 composite. Samples showed prominent PEC water oxidation performance, exhibiting ten-fold photocurrent than unmodified TiO_2 under the same conditions. Moreover, long-term PEC water splitting test demonstrated that the photo-stability of IL-TiO_2 was greatly enhanced. Liu et al. [42] applied 1-butyl-3-methylimidazolium tetrafluoroborate [BMIM][BF_4] for anatase preparation by a low temperature hydrothermal method. The existence of [BMIM][BF_4] enhanced polycondensation and crystallization rate, which encouraged the formation of anatase crystal. The TiO_2 showed higher photocatalytic activity in the degradation of p-chlorophenol than that of the commercially available TiO_2, Degussa P25. The highly ordered TiO_2 nanorods was obtained by Peng et al. [43] in presence of 1-butyl-3-methylimidazolium bromide [BMIM][Br]. The presence of IL was found to be vital for the formation of rutile nanorods that were rectangular with width of 100–200 nm and length of more than 1 mm, and grew up typically along *c*-axis to form the arrays against the substrate. The nanorods of rutile titania was also obtained by Yu et al. [44] who used similar in structure IL that is 1-butyl-3-methylimidazolium chloride [BMIM][Cl]. It was proposed that the formation of rutile crystal phase was due to high acidity of the system and high Cl^- content in the reaction environment. The combination of the IL-templated effects with reaction limited aggregation resulted in the hierarchical nanostructure formation. Nagaraju [45] proposed usage of functionalized ILs N, *N*-diethyl, ethylamine methylimidazolium hydrogen chloride [DEAIM] for TiO_2 nanoparticles preparation. Transmission electron microscopy (TEM) analysis revealed that the primary nanoparticles are clustered to form larger agglomerates during the formation stage itself and size of the nanoparticles was found to be ~30 nm. FTIR spectra confirm a presence of IL on the surface of the nanostructures. Concluding, there is a deficiency of information concerning the role of ionic liquids (depend on the ILs structure) in the mechanism of TiO_2 particles formation/growing, as well as, in the mechanism of ILs-modified TiO_2 excitation.

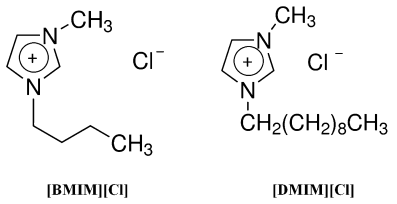

Fig. 1. The structure of 1-butyl-3-methylimidazolium chloride [BMIM][Cl] and 1-decyl-3-methylimidazolium chloride [DMIM][Cl].

In view of this, in the present paper we show the effect of the ionic liquid structure (the alkyl chain length in the cation) and the effect of the ionic liquid amount used during synthesis on the morphology, surface properties and photoactivity of the TiO_2 particles. To elucidate the influence of the IL structure, we chosen [BMIM][Cl] and 1-decyl-3-methylimidazolium chloride [DMIM][Cl] ionic liquids (shown in Fig. 1). Thus, it is a first paper dealing with the morphology and surface composition of TiO_2 particles, obtained in the presence of different molar ratio of [BMIM] and [DMIM], in relation to their photocatalytic performance as well as ability to form hydroxyl radical, based on detection of fluorescent product of coumarine hydroxylation. Finally, based on the experimental studies the role of ion liquids in TiO_2 spheres stabilization as well as the role of ILs in photoactivity enhancement is proposed.

2. Experimental materials and methods

2.1. Materials

Titanium *n*-butoxide (TBOT) as a precursor of TiO_2 microparticles, hydrochloric acid as pH stabilizer and ethanol as reaction medium was provided by Sigma–Aldrich, and used as received. Ionic liquids 1-butyl-3-methylimidazolium chloride [BMIM][Cl] and 1-decyl-3-methylimidazolium chloride [DMIM][Cl], with purity of ≥99%, were purchased from Merck. Before use, ILs were degassed and dried under vacuum of 20 Pa (Thermo VT6025, Germany) for 24 h at temperature of 80 °C, to reduce water and volatile compounds content to negligible values. The water contents of these ILs were determined by coulometric Karl-Fischer titration (model 899 Coulometer, Metrohm). The water content in the ionic liquids was less than 300 ppm.

2.2. Preparation of IL-assisted TiO_2 particles

The IL-assisted TiO_2 particles were synthesized as follows: titanium (IV) n-butoxide (TBOT) was dissolved in an absolute ethanol under vigorous stirring, then hydrochloric acid, distilled water and ionic liquid were added. Various molar ratios of both ILs to TBOT (IL:TBOT) were chosen as listed in Table 1. After homogenizing, mixture was transferred to a 200 ml Teflon-lined stainless steel autoclave at 160, 180 or 200 °C for 4, 12 or 24 h. When reaction was completed, autoclave was cooled to room temperature, the product was washed with ethanol and deionized water and dried at 50 °C for 6 h. For comparison, reference TiO_2 was prepared using the same method without IL addition. The reaction yield refers the percentage yield, which serves to measure the effectiveness of preparation procedure and was calculated by dividing the amount of the desired product obtained during synthesis by the theoretical yield (see Eq. (1)). The theoretical yield was predicted by a stoichiometric calculation based on the number of moles of all reactants present.

$$\text{percent yield} = \frac{\text{actual yield}}{\text{theoretical yield}} \times 100\% \quad (1)$$

2.3. Surface properties characterization

The Rigaku-Ultima + diffractometer with Cu target (λ = 1.542 Å) equipped with graphite monochromator using copper Kα radiation (40 kV tube voltage and 20 mA tube current) operating in the Bragg–Brentano geometry was used for X-ray diffraction analysis (XRD). The freshly grinded powder was homogeneously spread on the micro cover glass holder of *ca.* 0.2 mm depth. The crystal structure of the IL-TiO_2 particles was determined from XRD pattern measurement on the range of 2Θ = 20–70°, with the scan speed 0.3°/min.

The morphology of the semiconductors was investigated by scanning electron microscopy (SEM) technique using Hitachi Microscope TM-1000 under high vacuum with accelerating voltage 15 kV. TEM analysis were performed on the FEI Tecnai F20 X-Twin microscope. The samples were observed under bright-field (BF STEM) and SE mode (detection of secondary electrons, information about the morphology of the surface). Samples were suspended in ethanol (99,8%) and put into a ultrasonic bath (InterSonic IS-1K) for 5 s. Then, the drop (4 μl) was collected and placed on a copper mesh coated with a layer of carbon with holes (Plano, typ Lacey Cu 400 mesh). The solvent was evaporated at room temperature.

The surface area of the samples were evaluated from the adsorption–desorption isotherms of liquid nitrogen (77 K) detected using a Micromeritics Gemini V200 Shimadzu equipped the VacPrep 061 Degasser. The photocatalyst samples were dried and degassed in a sample cell at 200 °C for at last 2 h before adsorption. The specific surface areas of the photocatalysts were determined by Brunauer–Emmett–Teller (BET) method in the relative pressure range (p/p_0) 0.05–0.3.

For determination of the elemental composition of the synthesized materials CHNS analyzer model Thermo Scientific Flash 2000 was used working with a combustion furnace temperature of about 1000 °C.

Surface composition characterization of the IL-assisted TiO_2 particles was achieved by X-ray photoelectron spectroscopy (XPS) using a PHI 5000 VersaProbe^{TM}(ULVAC-PHI) spectrometer with monochromatic Al Kα radiation (h = 1486.6 eV). X-ray beam was focused to diameter 100 μm, measured area was defined as a 250 μm square. The high-resolution (HR) XPS spectra were collected with the hemispherical analyzer at the pass energy of 23.5 eV, the energy step size of 0.1 eV and the photoelectron take off angle 45° with respect to the surface plane. The CasaXPS software was used to evaluate the XPS data. Deconvolution of HR XPS spectra were performed using a Shirley background and a Gaussian peak shape with 30% Lorentzian character. The binding energy (BE) scale of all detected spectra was referenced by setting the BE of Ti $2p_{3/2}$ signal to 458.6 eV.

2.4. Measurement of photocatalytic activity

2.4.1. Phenol degradation

The photocatalytic activity of TiO_2 samples under UV–vis light was studied by measuring the rate of phenol decomposition in aqueous solution. Fifteen milliliter of photocatalysts suspension (7.5 mg) in phenol aqueous solution (0.43 mmol/dm^3) was placed in a quartz reaction tube. The mixture was stirred with a magnetic stirrer. After 30 min in the dark, the suspension was photoirradiated with high pressure Hg lamp (Heraeus, 150 W), which emits both UV and Vis light. The temperature of the suspension during photoirradiation was maintained at 10 ± 0,5 °C using a thermostatically controlled water bath. Aqueous suspension (0.15 cm^3) was collected at regular time periods (20 min.) during irradiation and filtered through syringe filters (Ø = 0.2 μm) to remove fine particles of the photocatalyst. Phenol concentration was determined by colorimetric method (λ_{max} = 480 nm) after derivatization with diazo-p-nitroaniline using UV–vis spectrophotometer (Evolution 220, Double-beam with Application Focused used Beam Geometry, Thermo-Scientific). Photocatalytic degradation runs were preceded by blind test in the absence of photocatalysts or illumination.

2.4.2. Formation of hydroxyl radicals

Formation of hydroxyl radicals were conducted in a cylindrical batch photoreactor equipped with quartz window, cooling system and 150 W Xenon lamp (Hamamatsu) as an irradiation source. Firstly, aqueous suspension containing 1 g/dm^3 of a photocatalyst and 10^{-3} M of coumarin were stirred magnetically and aerated (5 dm^3/h) for 30 min in the dark followed by 60 min irradiation. Aliquots of the suspension were collected at regular time periods (20 min) during irradiation and filtered through syringe filters (Ø = 0.2 μm). The fluorescence emission spectra of coumarin hydroxyproducts were conducted with 330 nm excitation, using Perkin Elmer LS50B Fluorescence Spectrometr.

3. Results and discussion

3.1. Selection of the synthesis conditions

In order to investigate the effect of time and temperature on the effectiveness, size and photocatalytic activity of the TiO_2 particles prepared by the IL-assisted solvothermal synthesis, experiments were performed with the IL:TBOT molar ratio of 1:10 at various

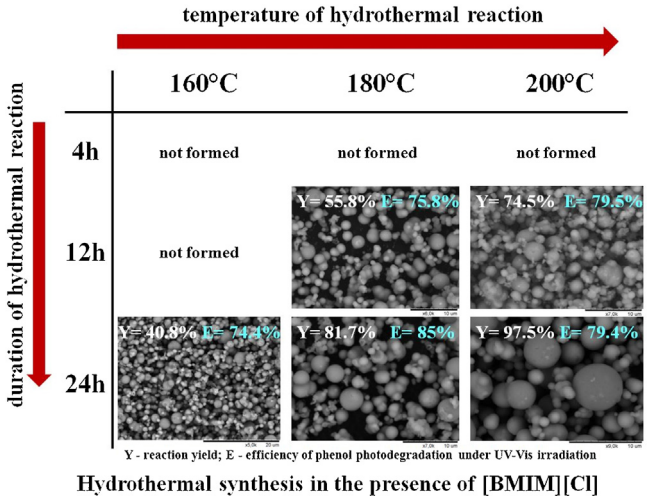

Fig. 2. The effect of BMIM-assisted solvothermal reaction conditions (duration and temperature) on the morphology, yield of TiO_2 formation and photoactivity of formed TiO_2.

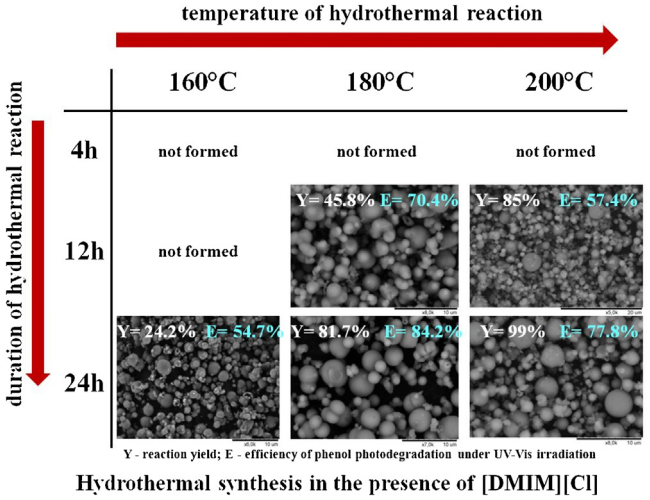

Fig. 3. The effect of DMIM-assisted solvothermal reaction conditions (duration and temperature) on the morphology, yield of TiO_2 formation and photoactivity of formed TiO_2.

temperatures 160, 180, 200 °C for 4, 12, and 24 h. The reaction process was supported by [BMIM][Cl] and [DMIM][Cl] ionic liquids for each reaction time and temperature.

It was observed that 4 h reaction time is not sufficient for effective TiO_2 nucleation and crystal growth regardless of the temperature as well as IL used in the experiment. Under these conditions neither no product or very little precipitate on the bottom of Teflon-lined autoclave was obtained. Increasing of the solvothermal treatment duration to 12 h, promotes TiO_2 particles formation, however only for syntheses carried out at temperature ≥180 °C for both [BMIM][Cl] and [DMIM][Cl] systems (Figs. 2 and 3). At 160 °C, only at 24 h reaction time of solvothermal reaction some products were shaped, nevertheless the reaction yields were low, 40.8% and 24.2% for [BMIM][Cl] and [DMIM][Cl], respectively. Well-developed spherical product was obtained at 180 and 200 °C when thermal treatment was set on 12 and 24 h. Therefore, prolongation of the synthesis time and increasing temperature facilitates microparticles formation that was observed as an increased reaction yield. Higher efficiency of the reaction was detected for mixtures containing ionic liquid with longer hydrocarbon chain [DMIM][Cl]. Increased reaction rate was also accompanied by a rise in the photocatalytic activity determined by measuring of the phenol decomposition. The highest photocatalytic activity was obtained for the TiO_2 particles prepared at 180 °C during 24 h in the presence of [BMIM][Cl] - 85% and [DMIM][Cl] –84.2% after 80 min of irradiation. Therefore, for further investigations of the ionic liquid influence on the morphology and photoactivity of TiO_2 photocatalyst the reaction temperature 180 °C and time 24 h were chosen.

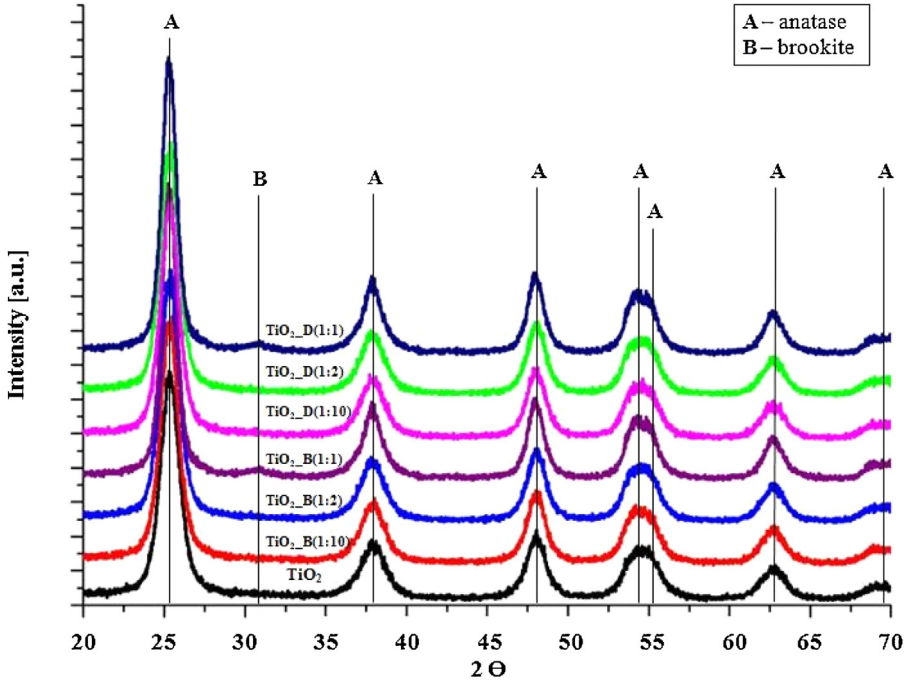

Fig. 4. XRD patterns of TiO_2 synthesized using various molar ratios of IL to TBOT.

Table 2
NCHS analysis of as-prepared TiO_2 photocatalysts obtained by ILs-assisted solvothermal route.

Sample label	Elemental composition (wt.%)			
	N	C	H	S
TiO_2	0.27	0.37	0.92	0
TiO_2_B(1:10)	0.01	0.40	1.08	0
TiO_2_B(1:2)	0.01	0.33	1.03	0
TiO_2_B(1:1)	0.04	0.68	0.91	0
TiO_2_D(1:10)	0.01	0.40	1.10	0
TiO_2_D(1:2)	0.01	0.38	1.00	0
TiO_2_D(1:1)	0.06	0.64	0.74	0

3.2. Crystal structure and morphology

Power X-ray diffraction analysis was used to verify the crystalline phase and estimate crystallite sizes of the synthesized TiO_2 particles (Fig. 4). For all samples, a set of diffraction peaks at 2Θ values of 25.3°, 37.7°, 48°, 54°, 55°, 63° and 68.5° were detected, which are attributed to anatase phase formation. As shown in Fig. 4, trace impurities identified as brookite were present in the samples where IL:TBOT molar ratio was 1:1. The average crystallite sizes of the particles, determined using Scherrer's equation, was observed to be in a range between 6.6 and 10.1 nm (Table 1). Addition of the ionic liquids to the reaction mixture provides particles with larger crystallites in comparison with samples prepared without ILs. The TiO_2 particles prepared in the IL:TBOT molar ratio 1:10 and 1:2 contain crystallites of average size 7.2 and 8.4 nm for [BMIM][Cl] and [DMIM][Cl], respectively. Increase in the IL content (IL:TBOT molar ratio 1:1) provides particles with even bigger crystallite sizes close to 10 nm.

The scanning electron microscopy images of the IL-assisted TiO_2 obtained in various IL:TBOT molar ratio (1:10, 1:2, and 1:1) in the presence of [BMIM][Cl] and [DMIM][Cl] are presented in Figs. 5 and 6, respectively. In order to compare, the SEM image of the reference TiO_2 particles is also included. It was revealed that the samples with the IL:TBOT molar ratio 1:10 and 1:2 as well as pristine TiO_2 particles have spherical structure. Moreover, TiO_2_[BMIM][Cl] particles have more regular shapes and more smooth surface then pristine TiO_2. That may indicate the ionic liquids ability to work as a structuring agent. However, for 1:1 IL:TBOT molar ratio the TiO_2 particles were poorly formed and had highly irregular shapes, indicating that the IL content was not sufficient to promote spherical structure formation, and additionally prevents uniform growth of the particle. This observation demonstrates that amount of the IL plays a crucial role in the formation of the TiO_2 microspheres.

Particle size distribution, performed by counting diameters of at least one hundred particles, reveals microstructures ranging from 1 to 6 μm. The pristine TiO_2 photocatalyst is formed mainly by particles with sizes ranging from 1 to 4 μm, with the higher contribution of the 1–3 μm particles (Fig. 5a). Introduction of the ionic liquids provides microstructures with lower particles constituting main fractional range. The TiO_2 prepared in the presence of [BMIM][Cl] (1:10 molar ratio) formed mainly particles with diameter 0.5–1 μm (44%). In the case of [DMIM][Cl], for both molar ratios 1:10 and 1:2 (Fig. 6a and b), higher contribution have structures with diameter of 1–2 μm (~50%). That observation may confirm structuring role of the ILs as well as ability to form a protective layer on the surface of the growing structures, therefore ability to control particle growth and inhibit further agglomeration. Based on the experimental results, a possible formation mechanism is presented in the next part of this article.

The TEM micrographs of sample TiO_2_B(1:10) shown in Fig. 7, gave a bright observation of the samples in which the particles were comprised of inter-aggregated crystals with a diameter about

Table 3
Elemental composition (in at.%) and chemical characters of carbon states in the surface layer of pristine TiO_2 and [BMIM]/[DMIM]-assisted TiO_2 particles, evaluated by XPS analysis.

Sample label	∑Ti (at.%)	Fraction Ti state		∑O (at.%)	Fraction O state			∑C (at.%)	Fraction C state			∑N (at.%)	∑Cl (at.%)	N/Ti
		Ti^{4+} 458.6 eV (%)	Ti^{3+} 457 eV (%)		TiO_{latt} 529.7 eV (%)	TiO_{surf} 530.4 eV (%)	OH 531.3 eV (%)	CO, TiON 532.4 eV (%)	"A" (C-C) 284.6 eV (%)	"B" (COH, NCCN) 286.2 eV (%)	"C" (C=O, N—C=N) 288.8 eV (%)			
TiO_2	29.44	97.59	2.41	66.27	62.35	28.60	6.59	2.46	4.15	72.27	13.46	14.27	0.14	0.00	0.0048
TiO_2_B(1:10)	27.43	92.59	7.41	61.40	71.15	21.28	6.20	1.37	11.16	66.04	29.96	4.01	0.15	0.27	0.0055
TiO_2_B(1:2)	26.94	93.84	6.16	61.84	74.08	17.59	6.08	2.25	10.92	65.44	28.49	6.06	0.19	0.10	0.0071
TiO_2_B(1:1)	26.22	91.72	8.28	60.94	76.19	15.13	6.62	2.07	11.99	66.46	30.21	3.33	0.22	0.63	0.0084
TiO_2_D(1:10)	26.39	92.02	7.98	61.56	71.55	19.41	7.33	1.72	11.89	64.67	31.23	4.10	0.06	0.11	0.0023
TiO_2_D(1:2)	26.28	91.84	8.16	61.11	69.40	21.14	7.45	2.01	12.47	65.11	30.45	4.44	0.09	0.06	0.0034
TiO_2_D(1:1)	26.31	93.03	6.97	61.63	66.65	23.91	7.29	2.15	11.20	64.98	30.69	4.33	0.22	0.64	0.0084

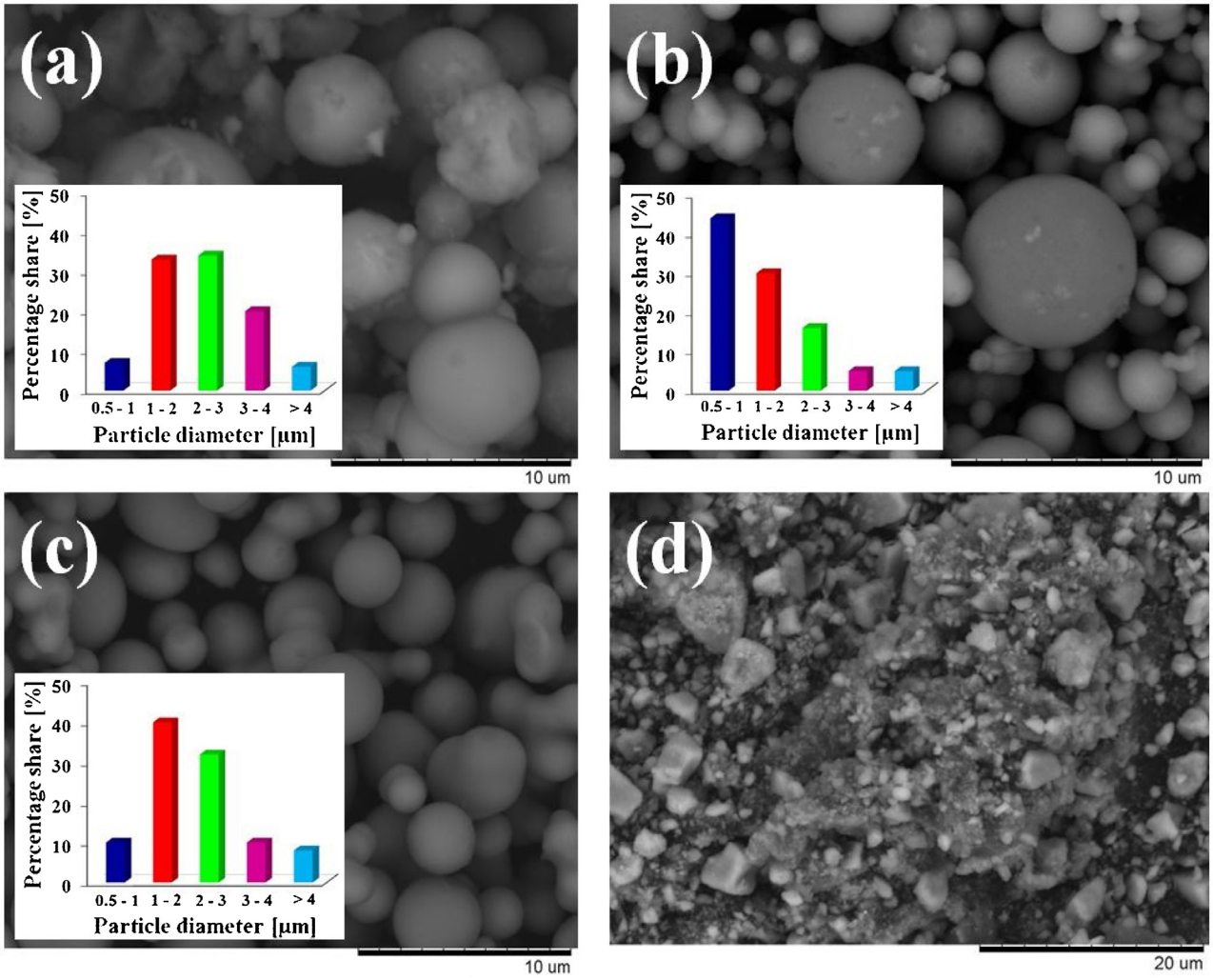

Fig. 5. SEM images and particle size distribution of TiO_2 obtained by solvothermal process (a) without IL, (b) with [BMIM][Cl] 1:10, (c) with [BMIM][Cl] 1:2, (d) with [BMIM][Cl] 1:1.

7.3 nm. The diameters of crystals estimated from TEM images confirm the average crystal size (7.2 nm) calculated based on the peak broadening using the Scherrer formula. It could be also observed that the IL-assisted TiO_2 microspheres are not hollow, which provides additional information about possible formation mechanism.

3.3. BET surface area

The BET surface areas determined for the IL-assisted TiO_2 photocatalysts are listed in Table 1. Depending on the type of the ionic liquid, as well as IL:TBOT molar ratio the surface area of the TiO_2 particles varied from 188 to 218 $m^2\,g^{-1}$ and was higher than detected for pristine TiO_2 microparticles (184 m^2/g). Influence of the imidazolium substituent chain length on the surface properties was also noticed that may reveal dependence of the specific surface area on the hydrophobicity of the TiO_2 surface due to IL adsorption. Generally, photocatalysts obtained during [DMIM][Cl]-assisted solvothermal synthesis had higher specific areas then those achieved by application of the ionic liquid with shorten alkyl substituent. The IL adsorption on the TiO_2 surface occurs, indeed, and will be discussed in the next section (3.4.).

In addition, increasing of the IL content in the reaction mixture from 1:10 to 1:2 IL:TBOT molar ratio also provides particles with higher surface area. The highest surface area (218 $m^2\,g^{-1}$) was observed for the sample TiO_2_D(1:2). Above this concentration BET surface area significantly decreased (188 $m^2\,g^{-1}$–TiO_2_D(1:1)) or remained almost at the same level (201 $m^2\,g^{-1}$–TiO_2_B(1:1)). These observations indicated that using too high concentration of both [BMIM][Cl] and [DMIM][Cl] may result in overloading of the TiO_2 surface, preventing formation of the spherical microparticles with developed surface area [42]. These conclusions are in an agreement with abovementioned SEM results. Regardless of the IL structure increasing its concentration in the reaction mixture, provides particles with higher pore volume. Application of the IL with 1:1 IL:TBOT molar ratio led to increase of pore volume accompanied by a decrease of the specific area, which is probably due to the steric hindrance during growth of the TiO_2 crystallites via Ostwald ripening [44]. Dependence of the IL structure and content on the particles composition will be further discussed in the following section.

3.4. Chemical composition of the IL-assisted TiO_2

Further information about the composition of the surface as well as bulk photocatalysts was provided by the XPS method and CHNS elemental analysis of the isolated particles. The CHNS analysis revealed the presence of carbon, nitrogen and hydrogen atoms in the compositions of the samples prepared in the presence as well as without ionic liquids (Table 2). The carbon, hydrogen and nitrogen peaks may be attributed to the residual ionic liquid present at

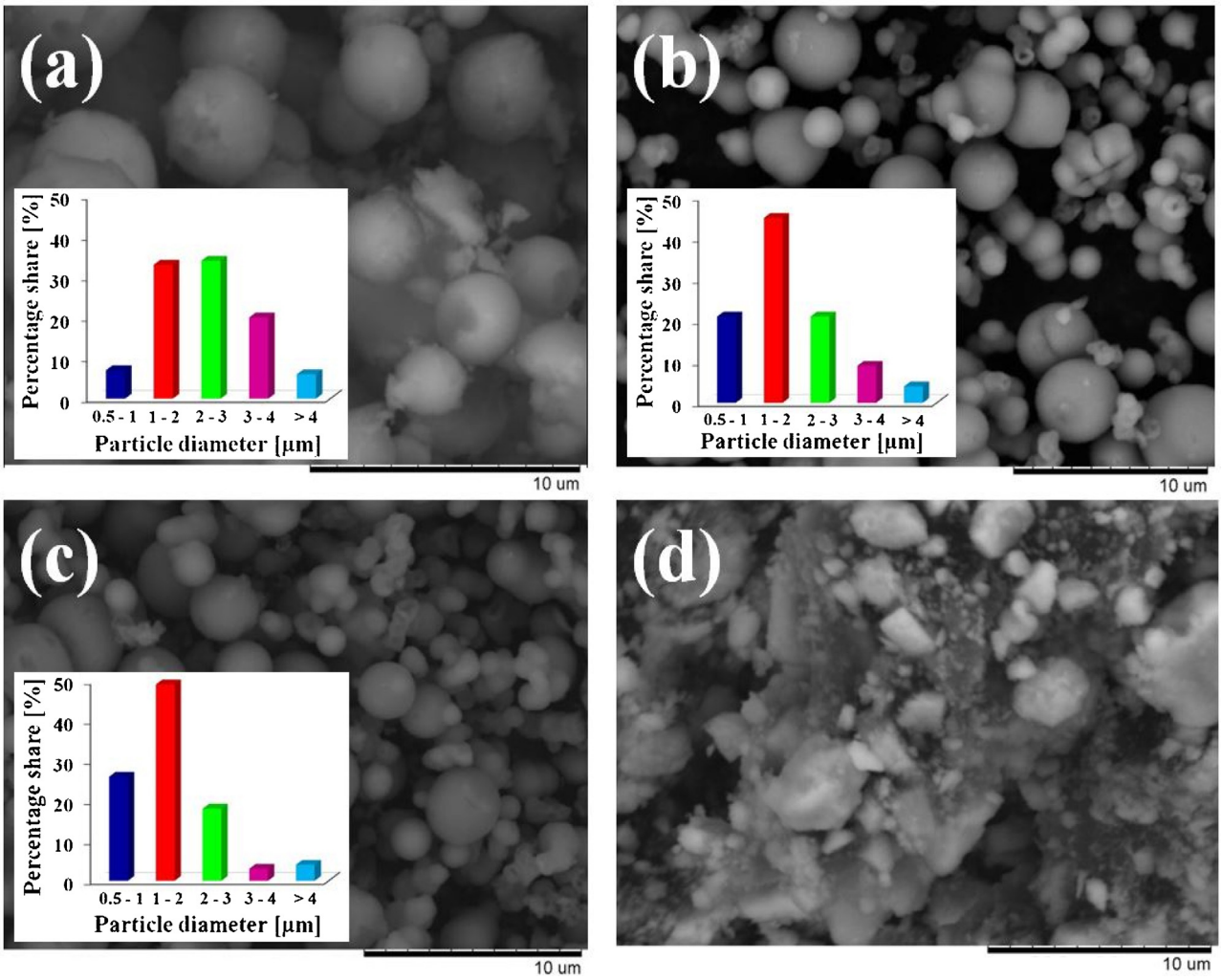

Fig. 6. SEM images and particle size distribution of TiO_2 obtained by solvothermal process (a) without IL, (b) [DMIM][Cl] 1:10, (c) with [DMIM][Cl] 1:2, (d) with [DMIM][Cl] 1:1.

the surface of the TiO_2 particles. However, detection of the CHN elements in the pristine TiO_2 sample may also indicate the presence of the impurities related with the samples preparation. Nevertheless, the higher IL content used in the synthesis, the higher amount of the carbon and nitrogen present in the particle composition. This results provide indication of the effective interaction of the imidazolium cation with the TiO_2 surface in a form of the protective layer. Despite plenty of work has been done to describe the type of interactions of the ionic liquids moieties with metal/semiconductor particle surface as well as structure of the protective IL layers formation, there is still controversial debate surrounding this area [9]. Therefore, more detailed information about the type of interaction of the TiO_2 particles via both cationic and anionic compartments of the ILs was obtained from XPS studies.

The HR spectra of Ti 2p, O1s, C1s, N1s and Cl 2p were recorded for all detected elements: titanium, oxygen, carbon, nitrogen and chlorine, respectively. The elemental surface composition of all IL-TiO_2 samples is presented in Table 3. The effect of the IL induced modification of TiO_2 microparticles was revealed by the recorded HR spectra of C 1s, N1s, Cl 2p (Fig. 8) and Ti 2p, O 1s (Fig. 9). The C 1s spectra were deconvoluted for three peaks, at binding energy (BE) of 284.5–284.7 eV, 286.1–286.3 eV and 288.7–288.9 eV (see carbon states "A", "B" and "C", respectively in Table 3). For TiO_2 sample these states can be assigned to CC (aromatic and aliphatic), C—OH, and C=O, respectively [46]. However, for the IL-assisted TiO_2 samples the last two carbon states can also be originated from chemisorbed imidazole. The "B" state (BE = 286.2 eV) is characteristic for N—C=C—N bound (imidazole-metal bound formed through C4 or C5 carbon in imidazole ring), whereas state "C" (BE = 288.8 eV) can be identified as N—C=N (imidazole-metal bound formed through C-2 carbon in imidazole ring) [47]. The XPS data presented in Table 3 revealed significant increase of relative contribution of state "B" and decrease of state "A" and "C" for all IL-assisted TiO_2 samples to compare with TiO_2 sample. On the other hand TiO_2_B(1:2) sample contain the highest amount of carbon in the form of N—C=N and C=O species (state "C") among all ILs-TiO_2 samples.

Nitrogen content in surface layers of TiO_2 samples prepared in presence of [BMIM[Cl] (TiO_2_B(1:10), TiO_2_B(1:2)) was estimated to be larger than in corresponding TiO_2_D(1:10) and TiO_2_D(1:2) (see Table 3). The atomic concentration ratio N/Ti values for TiO_2_B(1:10) and TiO_2_B(1:2) samples were found to be 2.4 and 2.1 times larger than for corresponding TiO_2_D(1:10) and TiO_2_D(1:2) samples, respectively (Table 3). Thus, assuming that nitrogen in both types TiO_2 specimens is originated mainly from IL interaction, we can conclude that the surface concentration of imidazole adspecies in [BMIM]-assisted TiO_2 is relatively larger than in corresponding [DMIM]-assisted TiO_2 samples.

Small concentration of nitrogen (Table 3) implicate low intensity N1s spectra for all IL-assisted TiO_2 samples (Fig. 8). Deconvo-

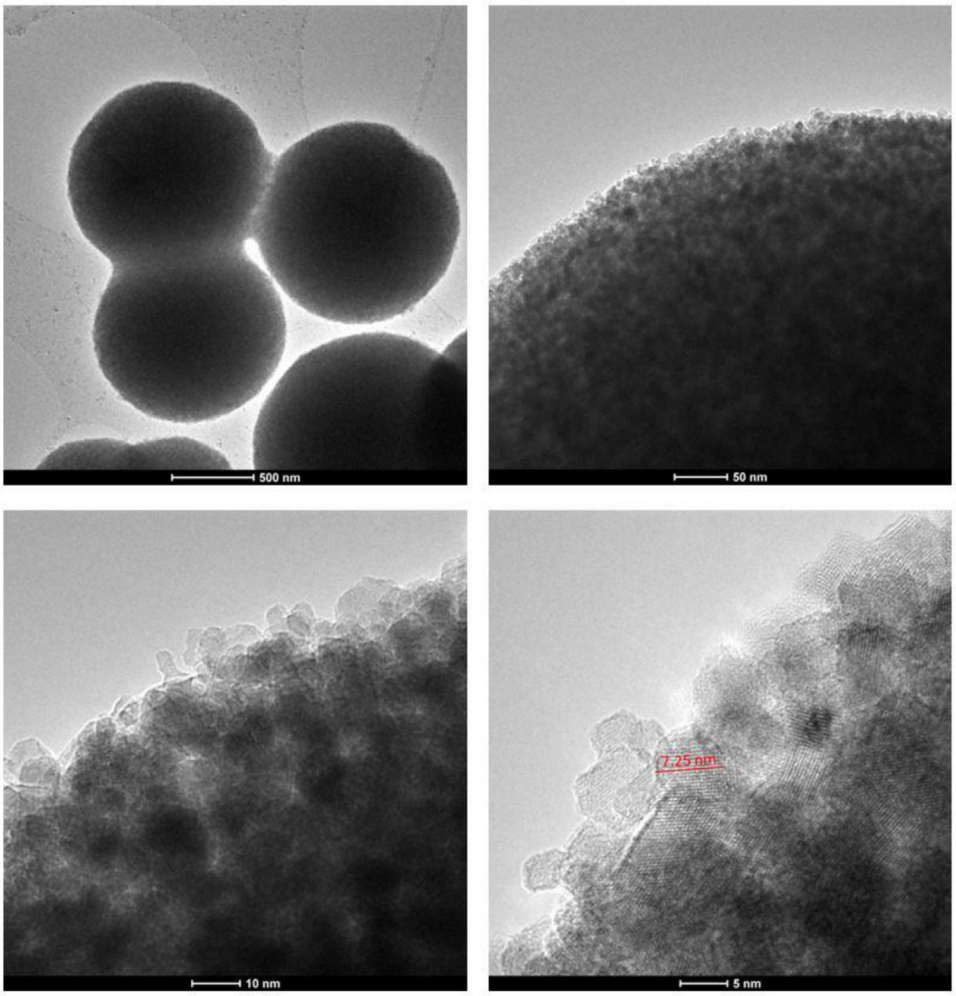

Fig. 7. TEM images of TiO_2 obtained in the presence of [BMIM][Cl] (sample TiO_2_B(1:10)).

lution of these spectra reveal two well distinguished nitrogen states located at BE of 399.6–400.2 eV and 401.4–401.5 eV, respectively. Similar N 1s spectra were reported for imidazole species chemisorbed on Ag [47–49]. Following these observations we can assume that the first broad peak, detected in all IL-assisted TiO_2 samples in Fig. 8, represents two coexisting nitrogen states formed by C—NH—C and C=N—C bounds, which are attributed to pyrrole- and pyridine-type interactions [47–49]. Unfortunately the nitrogen state at BE close to 400 eV is formed by various nitrogen compounds, including molecularly adsorbed nitrogen species [50,51]. Thus, the weak nitrogen peak detected on TiO_2 sample (Table 3 and Fig. 8) may result from the nitrogen species adsorbed on the surface of TiO_2 and cannot be the origin of IL interaction. It is likely that nitrogen contaminant species interaction with pristine TiO_2 leads to formation of Ti-O-N surface species, which are expected at BE close to 400 eV [51–53]. It also coincides with the O 1s spectra features for TiO_2, where contribution of oxygen state at BE about 532 eV, attributed to Ti—O—N adspecies formation [52], was found to be relatively larger than corresponding state detected for the IL-modified TiO_2 samples (Table 3). The peak at BE of 401.5 eV can be ascribe to the positively charged nitrogen ($-N^+$) [48,49] originated from pyridine–type nitrogen bound. It is interesting to note that the positively charged imidazole states appear mainly in TiO_2_B(1:1) and TiO_2_D(1:1) samples and are accompanied by relatively large coverage of chlorine species (Table 3 and Fig. 8). Decomposition of the Cl 2p spectra recorded on all IL-assisted TiO_2 samples reveal only one chemical state of chlorine represented by Cl $2p_{3/2}$ peak located at BE 198.1–198.5 eV, which can be assigned to TiClx adspecies [51]. It is highly probable that interaction of negatively polarized chlorine ions modify the electronic environment of imidazole admolecules adsorbed on the TiO_2 particles, leading to formation of its positively charged forms.

Two chemical states of titanium were separated in the Ti2p spectra recorded on TiO_2 and all IL-assisted TiO_2 samples (Fig. 9) at BE of Ti$2p_{3/2}$ peak close to 458.6 eV and 457 eV, which can be identified as Ti^{4+} and Ti^{3+} species, respectively [46]. Relative contribution of both states in all samples is specified in Table 3. One can see that content of Ti^{3+} state in all IL-assisted TiO_2 samples appeared to be much larger than in pristine TiO_2 sample what evidences the IL modification of TiO_2 surface. The Ti2p XPS spectra reported by Cong et al. [52] reveal decrease of BE for the Ti$2p_{3/2}$ peak from 459.05 eV to 458.25 eV as a result of nitrogen doping of pristine TiO_2. Probably we observe the same tendency of BE shift for surface specimens appearing as a result of the IL interaction with TiO_2.

Four oxygen states were separated in the O 1s spectra (Fig. 9) what agree well with deconvolution model reported in [54]. For our specimens we can relate the first peak at BE of 529.7 eV to the TiO_2 crystal lattice, the second at BE of 530.4 eV to the Ti—O surface species, the third at BE of 531.3 eV to —OH group and forth at BE of 532.4 eV to C—O bond. The last peak can be also interpreted as Ti—O—N or Ti—N—O bond formation [51,52,55,56].

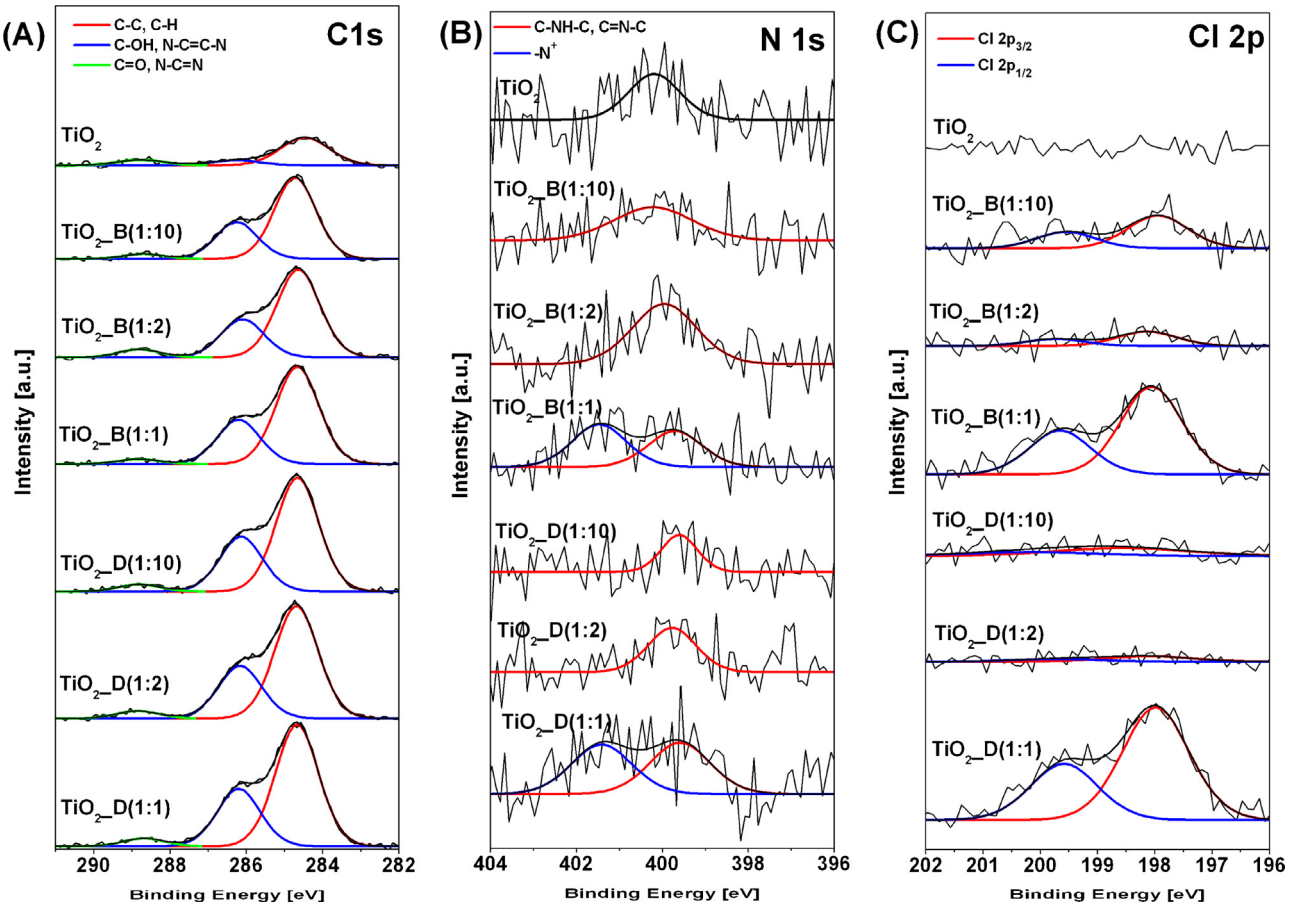

Fig. 8. XPS HR spectra of C1s, N 1s, Cl 2p of prepared photocatalysts TiO_2 assisted by ionic liquids.

3.5. Photocatalytic activity

The photocatalytic activity of as-prepared samples was investigated by determination of the phenol decomposition rate in the presence of UV–vis irradiation (Fig. 10) as well as 7-hydroxycoumarin formation rate related to concentration of OH radicals (Fig. 11). Phenol was chosen as a model contaminant, due to its toxicity towards higher organisms. Photolysis of phenol (without photocatalysts) under UV–vis illumination is also presented on the Fig. 10. Kinetics of phenol photodegradation in the aqueous solutions by the IL-assisted TiO_2 samples is shown in Table 1. Commercial P25 photocatalyst and pristine TiO_2 synthesized by solvothermal method without addition of the ionic liquid were used as the reference systems. It was found that samples with IL:TBOT molar ratio 1:10 and 1:2 revealed higher ability to phenol degradation than unmodified TiO_2 (Fig. 10). Phenol degradation rate increased from 5.2 to 5.3 and 5.9 $mmol \cdot dm^{-3} \cdot min^{-1}$ for pristine TiO_2 and samples TiO2_B(1:10) and TiO2_B(1:2), respectively. Therefore, the photodegradation efficiency increased with increase of the quantity of ionic liquid up to molar ratio 1:2. However, further increase of the ionic liquid used in the synthesis resulted in the opposite effect. Thus, after 80 min of irradiation, 92% of phenol degradation was denoted for the sample TiO2_B(1:2), whereas only 56% for samples TiO2_B(1:1). It may indicate that IL:TBOT molar ratio 1:2 applied in the reaction mixture is the highest terminal ratio which effect on improvement the photocatalytic activity. Similar relationship was obtained for [DMIM][Cl]. Nevertheless, the presence of [BMIM][Cl] was only slightly beneficial for UV-light activation of TiO_2 in comparison with [DMIM][Cl] (89% of phenol degradation for TiO2_D(1:2)). Comparing results obtained for samples prepared in the presence of IL:TBOT molar ratio 1:2, the phenol degradation rate was calculated to be 5.5 and 5.9 $mmol \cdot dm^{-3} \cdot min^{-1}$ for [DMIM][Cl] and [BMIM][Cl], respectively. It means that elongation of the alkyl chain length in the imidazolium ring of IL had no significant effect on the improvement of the photocatalytic properties of as-prepared TiO_2.

An UV–vis irradiation of coumarin in the presence of TiO_2_IL samples led to formation of 7-hydroxycoumarin in the system (Fig. 11). A remarkable peak localized around 456 nm represents intensively fluorescent product of coumarin hydroxylation. In all cases of 7-hydroxycoumarin creation, an increase of the irradiation time resulted in gradual growth of the peak intensity at 456 nm. The results indicated that the increased amount of •OH produced at the surface of excited TiO_2_[BMIM][Cl] samples well correlated with more efficient degradation of phenol. In both cases, the sample TiO_2_B(1:2) showed the highest activity. Moreover, the sample TiO_2_B(1:1) revealed a significantly lower formation of hydroxyl radicals. For samples TiO_2 prepared in the presence of [DMIM][Cl] the peak intensity at 456 nm was comparable with the peak characteristic for the reference TiO_2. Nevertheless, modification with [DMIM][Cl] leads to enhancement of the photocatalytic properties compared to pristine TiO_2 in case of the phenol degradation reaction. This discrepancy could result from different pathway of phenol photodegradation and formation of 7-hydroxycoumarin through reaction of coumarin with generated hydroxyl radicals on the surface of photocatalysts. Phenol disappearance could results from: (1) •OH attack on phenol molecule; (2) reaction of that molecule with holes photogenerated in titanium dioxide; and (3) by direct oxidation by oxygen dissolved in water [57]. The intensity of 7-hydroxycoumarin formation is solely depend and on the amount of OH radicals produced at the surface of excited TiO_2 [58].

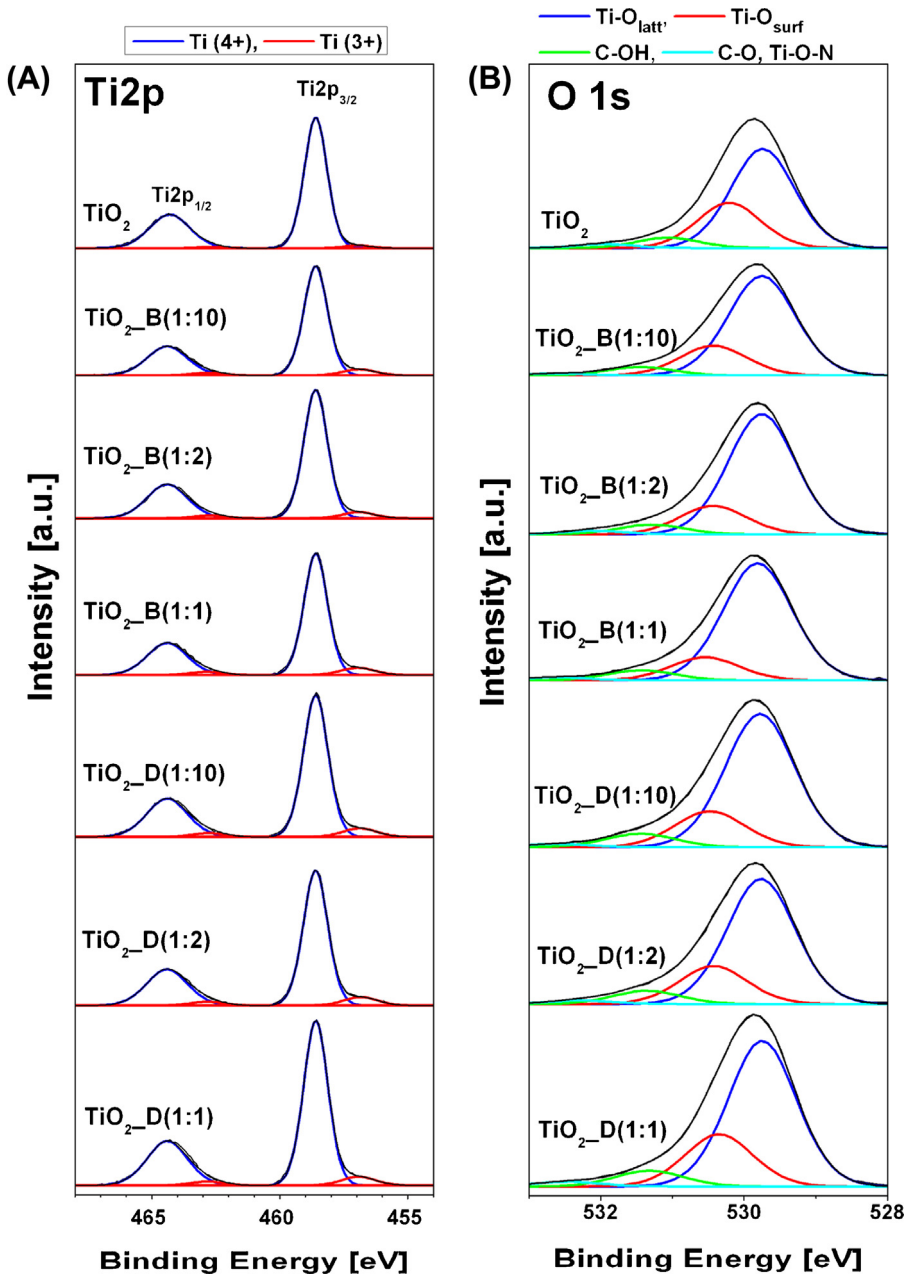

Fig. 9. XPS HR spectra of Ti 2p, O 1s of prepared photocatalysts TiO_2 assisted by ionic liquids.

3.6. Mechanism of the TiO_2 spheres formation

Precipitation of the TiO_2 particles in the solvothermal synthesis route begins with hydrolysis of the precursor (Fig. 12a) and formation and growth of the numerous small crystallites (nucleation). Some of the crystallites may adhere to the substrate whereas others may aggregate into spherical particles. Since particles aim to reduce the overall energy, molecules on the surface of small particles (being energetically unfavorable) detach from the particle, and diffuse into the solution. As a consequence, re-deposition of the smaller particles on the larger crystals according to Ostwald ripening mechanism take place and larger, more thermodynamically stable particles are formed. Growth of the particles is usually diffusion limited process, therefore factors influencing TiO_2 particles growth rate may be a structure as well as content of the ionic liquid used in the synthesis. Ionic liquids used in this study, being salts consisting of a large, asymmetric, amphiphilic imidazolium cation and Cl anions, interact with the TiO_2 surface forming protecting layer. Therefore, adsorption of the IL on the particles surface may results in the limiting of the smaller particles deposition, inhibiting growth and agglomeration (Fig. 12b). The [DMIM][Cl] ionic liquid film at the particle surface is probably less firmly packed since surface area occupied by one molecule of the amphiphilic compounds with longer alkyl chain may be higher due to steric hindrance and ability of the alkyl substituents to take a variety of arrangements. This conclusions is supported by XPS results where content of the nitrogen and chlorine atoms detected on the surface of TiO_2 prepared in the presence of [DMIM][Cl] was estimated to be smaller than in the surface layers of the corresponding [BMIM][Cl]-assisted TiO_2 particles. This ability may result in different interfacial properties when compared with [BMIM][Cl] system. Therefore, more compact film of the [BMIM][Cl] molecules formed at the particle surface may prevent smaller particles adhesion and aggregation providing particles with smaller size.

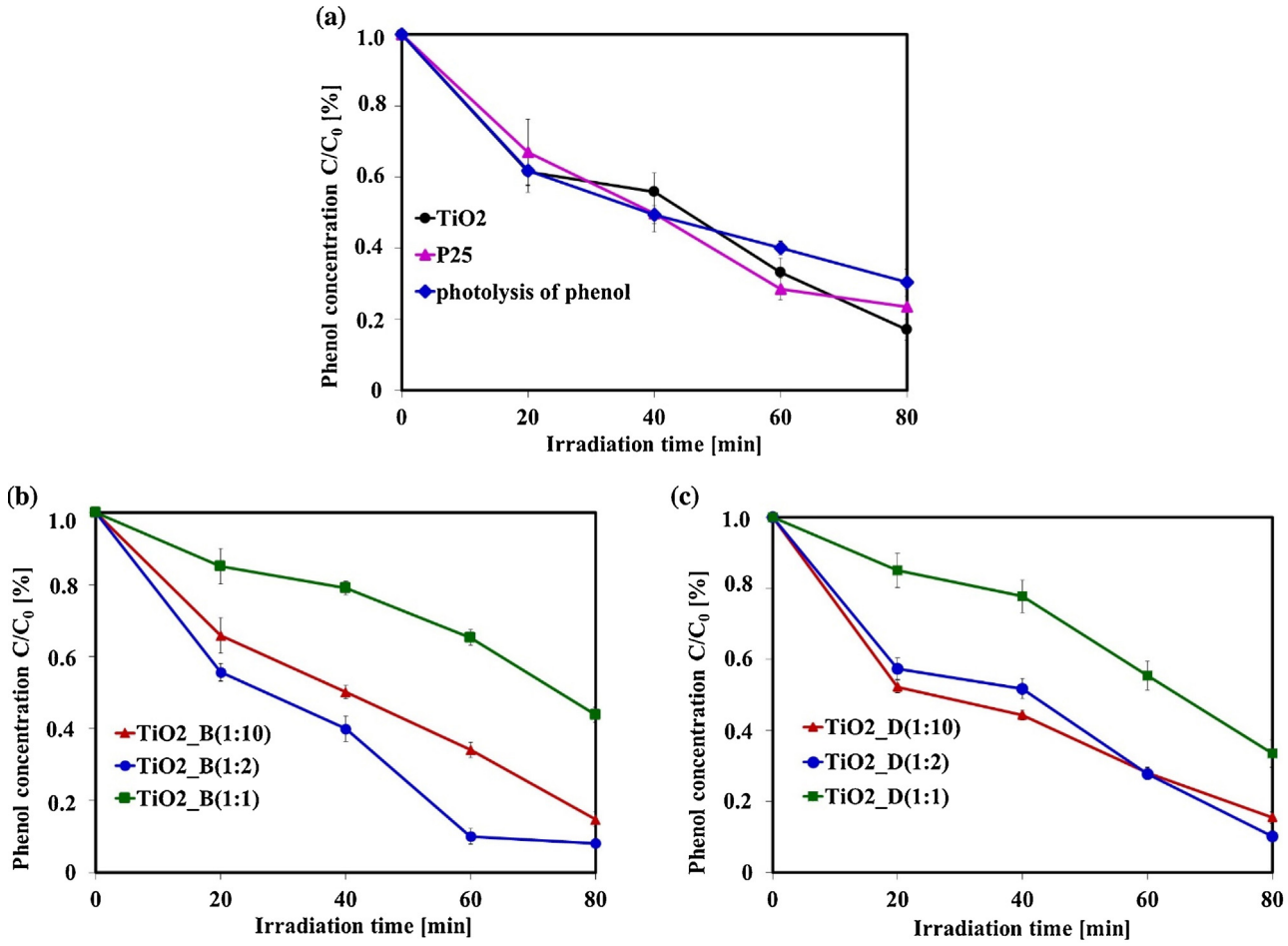

Fig. 10. Efficiency of phenol degradation under UV–vis light in the presence of (a) TiO_2, P25; (b) TiO_2 formed in the presence of [BMIM][Cl]; and (c) TiO_2 formed in the presence of [DMIM][Cl].

We can also conclude that parallel coordination of the TiO_2 particles by both imidazolium cation and anion, as ion pairs, take place. Both [BMIM] and [DMIM] cations interact with surface of the TiO_2 in a flat configuration, and the side alkyl chains of the cation are preferentially directed away from the particle surface. The electrostatic interactions provided by imidazolium cation is balanced by the chloride counter-ions. This means that ionic liquid definitely take part in the electrostatic stabilization of the TiO_2 particles, however that is not a sole type of interactions. Ionic liquid contain alkyl substituent that provide steric orientation on the surfaces being a consequence of the tendency of ILs to interact preferentially by the charge moieties of the ions, with nonpolar fragments directed away from the surface. The length of the hydrocarbon chain affects its conformation, and therefore ordering of the IL on the surface. In addition, ability of the IL moieties to form cation–cation and cation–anion interactions may facilitate formation of the uniform shell that surround TiO_2 surface. That means additional structural forces stabilizing TiO_2 microstructures [9].

Moreover, that protecting layer may take a form of a supramolecular structure composed of both cation and anion being in contact with the crystallites and particles. Elongation of the alkyl chain in the imidazolium cation may also result in aggregation of the alkyl substituent and as a consequence additional steric hindrance formation. In this regard, the overloaded film of ILs molecules may limit equal particles condensation on the TiO_2 surface. Moreover, taking into account that the rate of the nucleation step is high, whereas the Ostwald ripening processes remain relatively slow, preparation of the uniform, more regular shaped, spherical particles prepared in the IL:TBOT molar ration 1:1 is prohibited. Therefore, in order to prepare particles with required properties, ILs content has to be carefully selected.

3.7. Discussion of photocatalytic activity

The TiO_2 sample which exhibited best photoactivity under UV–vis light were prepared via IL-assisted solvothermal synthesis (180 °C, 12 h), using [BMIM][Cl] to TBOT molar ratio of 1–2. The TiO_2_B(1:2) sample is in anatase form with crystalline size ~7.2 nm and its surface area equals to 202 m^2/g. Phenol degradation rate increased from 5.2 and 5.5 to 5.9 mmol dm^{-3} min^{-1} for pristine TiO_2, TiO_2_D(1:2) and TiO_2_B(1:2), respectively (Table 1). Moreover, the highest efficiency of hydroxyl radicals formation was also observed for the TiO_2_B(1:2) sample. The TiO_2_B(1:2) sample consist of 24.94 at.% of Ti, 61.84 at.% of O, 10.92 at.% of C, 0.19 at.% of N, and 0.10 at.% of Cl. The XPS data clearly revealed that the amount of carbon in the form of N—C=N species (imidazole-metal bound formed through C-2 carbon in imidazole ring) correspond well with the change of the photoactivity (see details in Fig. 13a). The most active samples contained the highest amount of carbon in the form of N—C=N species among all ILs-TiO_2 samples. The apparent rate of phenol photodegradation increased up to 5.5 and 5.9 mmol dm^{-3} min^{-1} for samples containing 4.44 at.% (sample TiO_2_D(1:2)) and 6.06 at.% (sample TiO_2_B(1:2)) of carbon in "C' state. It should be noticed that the highest intensity of the

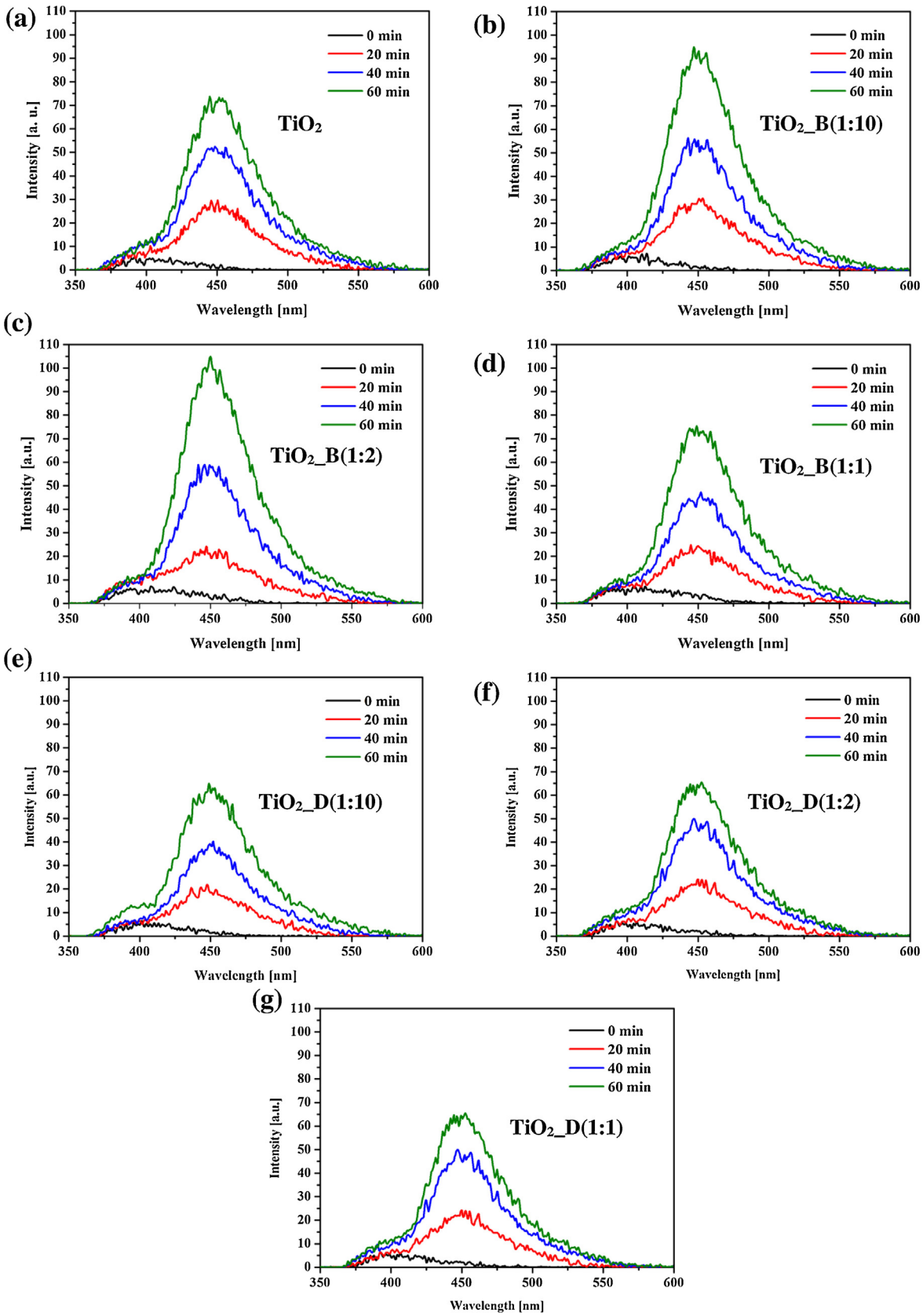

Fig. 11. Fluorescence spectra of irradiated coumarin solutions in the presence of (a) reference TiO_2; (b) TiO_2_B(1:10); (c) TiO_2_B(1:2); (d) TiO_2_B(1:1); (e) TiO_2_D(1:10); (f) TiO_2_D(1:2); (g) TiO_2_D(1:1).

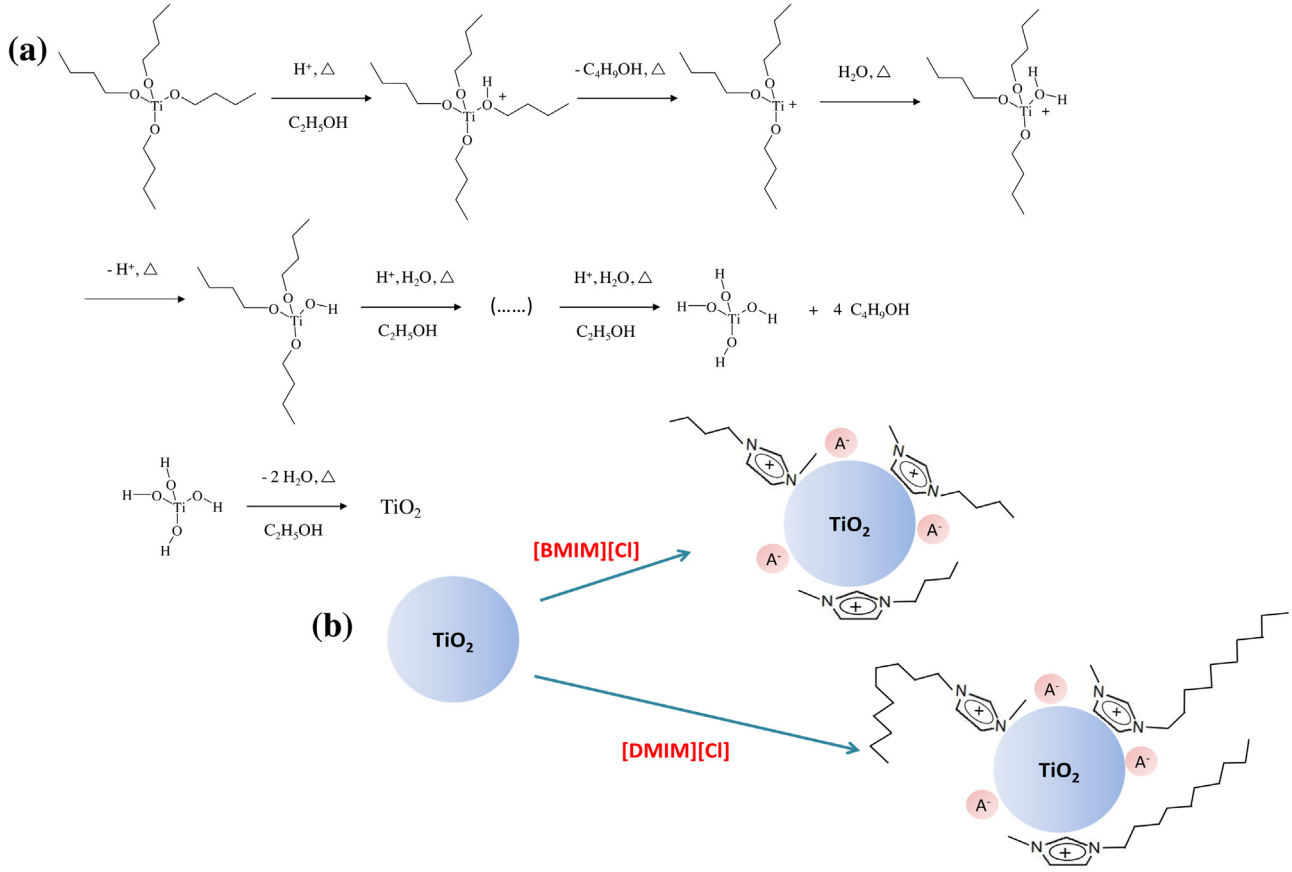

Fig. 12. Possible mechanism of TiO_2 spheres formation: (a) hydrolysis of TBOT, (b) the most important types of interaction of the imidazolium ions with TiO_2 particle providing colloidal stabilization.

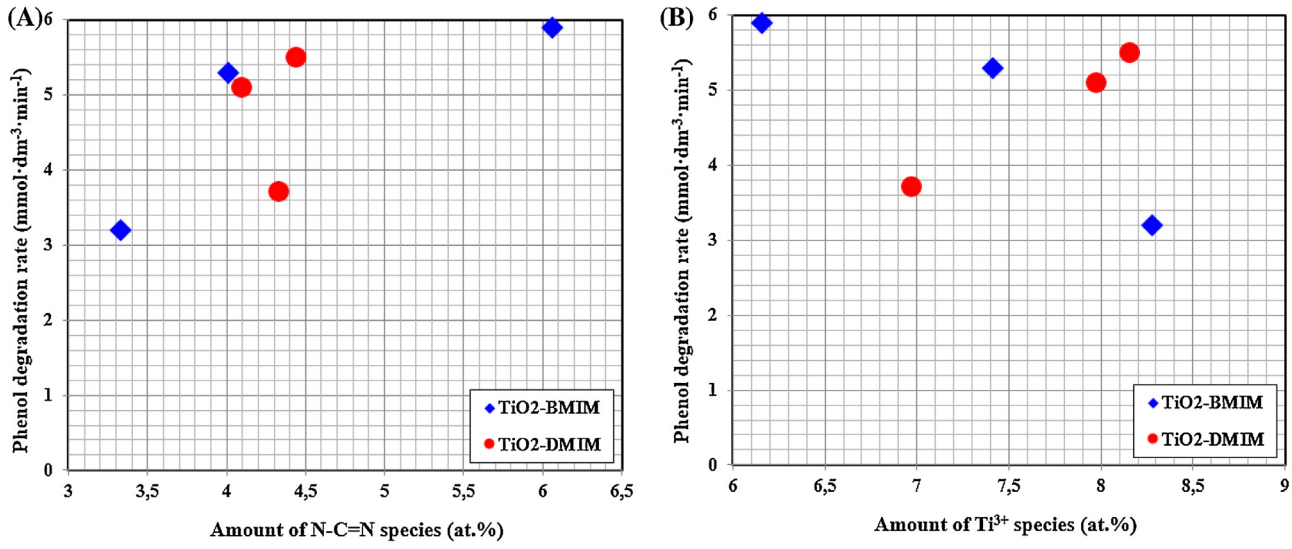

Fig. 13. Correlation between surface composition of ILs-TiO_2 particles and their photocatalytic activity in phenol degradation under UV–vis irradiation: (a) fraction of carbon species in the form of N—C=N, and (b) fraction of titanium species in the form of Ti^{3+}.

288.8 eV peak was observed for pristine TiO_2 (14.27 at.%), but this peak could be attributed both to the presence of C=O and N—C=N species. Thus, in case of bare titania the 288.8 eV peak could be attributed to the presence of C=O species, while in case of ILs-TiO_2 it could be ascribed mainly to the presence of N—C=N. It must be pointed that the amount of N—C=N species at the surface of TiO_2 particles are not dependent on the amount of ionic liquids introduced during solvothermal synthesis. For both ionic liquids, increase in ratio of ILs to TBOT from 1:10 to 1:2 resulted also in increasing amount of N—C=N species. However, continued augmentation of ILs amount (up to ILs: TBOT = 1:1) caused to decrease of detected amount of N—C=N species together with the distortion of spherical morphology and downfall of photoactivity. Moreover, the atomic concentration ratio N/Ti value for TiO_2-B(1:2)

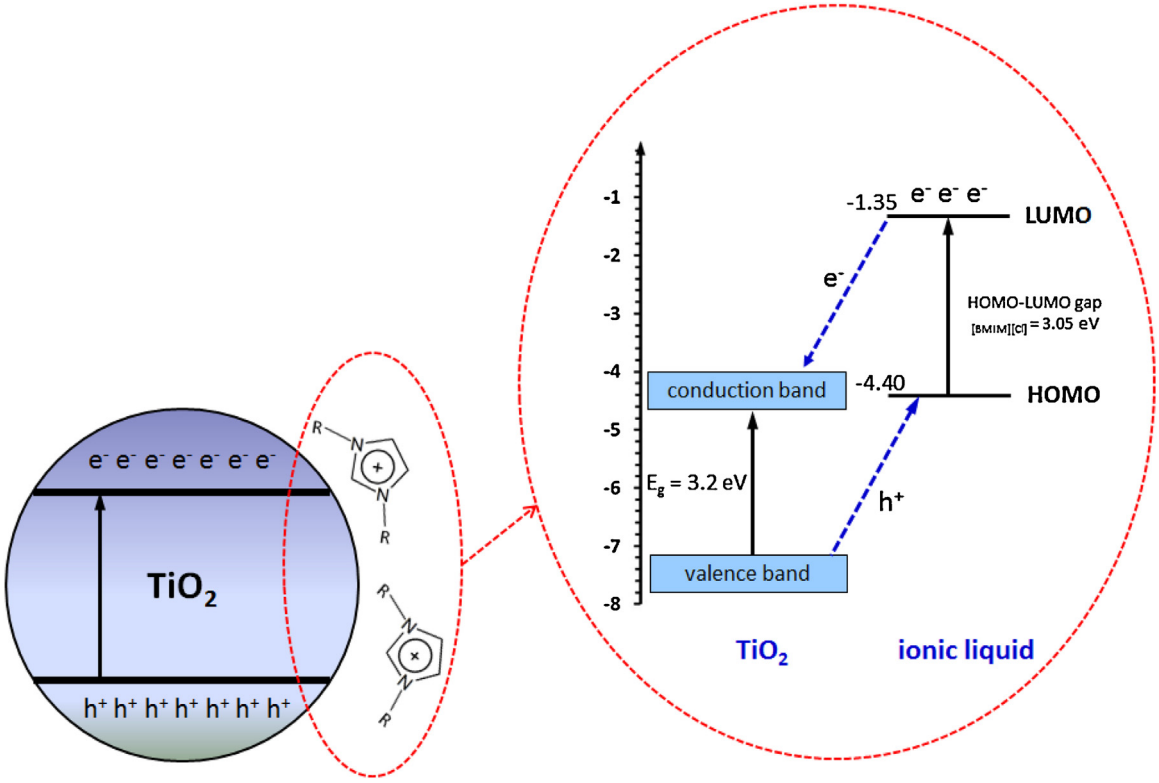

Fig. 14. A proposed mechanism of ILs-TiO_2 excitation under UV–vis light.

sample was found to be 2.1 times larger than for corresponding TiO_2_D(1:2), respectively (Table 3). Thus, the surface concentration of imidazole adspecies in [BMIM]-assisted TiO_2 is relatively larger than in corresponding [DMIM]-assisted TiO_2 samples, which could also affect improvement of photoactivity of TiO_2_B(1:2). Additionally, the UV–vis activity of the IL-assisted TiO_2 could be intensified by higher amount of carbon in comparison to pristine TiO_2 (Table 3) [46,59].

Furthermore, UV–vis activity of samples modified by ionic liquids could be enhanced by higher content of Ti^{3+} state compared to bare TiO_2 (Table 3). The correlation between the content of Ti^{3+} species in the surface layer of TiO_2 and UV–vis induced photoactivity is presented in Fig. 13b. Considering the effect of Ti^{3+} amount on the photocatalytic activity, the rate of phenol degradation drop from 5.9 to 3.2 mmol·dm^{-3}·min^{-1} when the amount of Ti^{3+} growth from 6.16 to 8.28 at.% for [BMIM]-assisted TiO_2. The opposite correlation was observed when [DMIM] was used for TiO_2 preparation. Rise of Ti^{3+} amount from 6.97 to 8.16 at.% led to suppression of photocatalytic activity. Nonetheless, for both samples obtained with a molar ratio IL:TBOT (1: 1) the activity was greatly reduced by poorly formed structure and irregular shapes of particles (ionic liquid prevented uniform growth of particles).

Liu et al. [42] reported enhancement of photocatalytic activity TiO_2 modified by [BMIM][BF_4] by increase of the BET surface area, good anatase crystal mesostructure and small crystal size. Increased of photoactivity of [ABsIM][HSO_4]-assisted TiO_2 was assumed by the synergistic effect between IL and TiO_2 resulting in a high charge separation rate based on the electron transfer and efficient electron extraction [41]. Thus, based on the obtained results and literature data, we propose a feasible mechanism to explain the upgrading photoactivity of the ILs-TiO_2 compare to the pristine one Fig. 14). As an ionic liquid molecule absorbs a photon with an appropriate energy, an electron is excited from the highest occupied molecular orbital (HOMO) to the lowest unoccupied molecular orbital (LUMO). Afterwards, the electrons could be transferred from the LUMO level of ionic liquid into the conduction band (CB) of the TiO_2 semiconductor. It should be indicated that the LUMO level has to be located higher in energy than CB to transfer an electron from the IL molecule into the semiconductor. The uncreative but coordinating environment and wide electrochemical window of imidazolium-based ionic liquids have been accounted by the strong donating electron character of the imidazolium-based ionic liquids [60]. The HOMO–LUMO gap of [BMIM][Cl] is 3.05 eV [61]. On the other hand, under the UV light illumination, electrons are excited from VB of TiO_2 to CB of TiO_2 to generate electron-hole pairs and generated holes could be directly injected into the HOMO level of IL.

4. Conclusion

The anatase TiO_2 microparticles were prepared by the ionic liquids assisted solvothermal method. Experiments were performed with different IL:TBOT molar ratio at various temperatures 160, 180, 200 °C and reaction time 4, 12, and 24 h and was supported by 1-butyl-3-methylimidazolium chloride [BMIM][Cl] and 1-decyl-3-methylimidazolium chloride [DMIM][Cl] ionic liquids. The temperature, duration of the solvothermal treatment as well as structure and quantity of the ionic liquid were observed to be essential factors in promoting the TiO_2 nucleation and crystal growth. Prolongation of the synthesis time, increasing the temperature, and addition of the ionic liquid with longer hydrocarbon chain [DMIM][Cl] facilitates microparticles formation with increased reaction yield. Moreover, application of the ionic liquids as a component of the reaction mixture (up to IL:TBOT molar ratio 1:2) results in formation of the smaller particles with larger crystallites, higher specific areas, more regular spherical shape, more smooth surface and less polydispersive then reference TiO_2 prepared without ILs. The effective interactions between ionic liquid components (carbon, nitrogen, hydrogen and chlorine) and microparticles surface was clearly demonstrated by the XPS and

CHNS analysis confirming external IL layers around the microparticles. Nitrogen and chlorine content in surface layers of TiO_2 prepared in the presence of [BMIM][Cl] was estimated to be larger than in corresponding TiO_2-[DMIM] species. Therefore, morphology and properties of the IL-assisted TiO_2 may be related with ability of ILs to adsorb at the TiO_2 surface and play a role of the structuring agent, controlling particle growth and inhibiting further agglomeration due to ionic liquids high dielectric constant and polarity, amphiphilic characteristics as well as inherent charge. However, overloaded of the particles with ionic liquid component impede uniform growth of the particles providing particles with highly irregular shapes as it was revealed for samples where IL:TBOT molar ratio was 1:1. Interestingly, in these samples the positively charged imidazole states were observed being accompanied by relatively large coverage of negatively polarized chlorine species. These observations demonstrate crucial role of the amount and structure of the ionic salts in the formation of TiO_2 microspheres.

Based on the XPS analysis, we can concluded that the presence of N—C═N, originated from imidazole ring, at the surface of TiO_2 is beneficial for the UV–vis photocatalytic activity. It should be also pointed out that the amount of carbon in the form of N—C═N species is depend not only on the type of ionic liquids but also on the amount of ILs used during the preparation route. Thus, ionic liquids could serve either as a stabilizing agent during TiO_2 particle formation as well as a molecule improving TiO_2 photoactivity. In addition, presence of the IL on the TiO_2 surface probably results in absorption of the photons and excitation of the electrons from HOMO to LUMO orbitals. Mechanism of the photoexcitation could be therefore related with transfer of the electron from the LUMO level of IL to the TiO_2 semiconductor conduction band.

Acknowledgements

The author J.Ł. acknowledges funding from the National Science Center within program OPUS 3 (grant entitled: Study on aggregation behavior of nonionic surfactants in ionic liquids, contract No. UMO-2012/05/B/ST4/02023). The author A.Z.M. acknowledges funding from the National Science Centre within program OPUS 2 (grant entitled: Preparation and characteristics of novel three-dimensional semiconductor-based nanostructures using a template-free methods, contract No.: UMO-2011/03/B/ST5/03243), for work described here.

Appendix A. Supplementary data

Supplementary data associated with this article can be found, in the online version, at http://dx.doi.org/10.1016/j.apcatb.2015.11.019.

References

[1] X. Chen, S.S. Mao, Chem. Rev. 107 (2007) 2891–2959.
[2] H. Li, X. Duan, G. Liu, X. Jia, X. Liu, Mater. Lett. 62 (2008) 4035–4037.
[3] S. Pavasupree, J. Jitputti, S. Ngamsinlapasathian, S. Yoshikawa, Mater. Res. Bull. 43 (2008) 149–157.
[4] U. Diebold, Surf. Sci. Rep. 48 (2003) 53–229.
[5] O.-O. Prieto-Mahaney, N. Murakami, R. Abe, B. Ohtani, Chem. Lett. 38 (2009) 238–239.
[6] B.K. Mutuma, G.N. Shao, W.D. Kim, H.T. Kim, J. Colloid Interface Sci. 442 (2015) 1–7.
[7] V. Žunič, M. Vukomanović, S.D. Škapin, D. Suvorov, J. Kovač, Ultrason. Sonochem. 21 (2014) 367–375.
[8] D. Fattakhova-Rohlfing, A. Zaleska, T. Bein, Chem. Rev. 114 (2014) 9487–9558.
[9] J. Łuczak, M. Paszkiewicz, A. Krukowska, A. Malankowska, A. Zaleska-Medynska, Adv. Colloid Interfac Sci. (2015), http://dx.doi.org/10.1016/j.cis.2015.08.006, accepted.
[10] J. Łuczak, M. Paszkiewicz, A. Krukowska, A. Malankowska, A. Zaleska-Medynska, Adv. Colloid Interfac Sci. (2015), http://dx.doi.org/10.1016/j.cis.2015.08.010, accepted.
[11] N.L. Mai, K. Ahn, Y.-M. Koo, Process Biochem. 49 (2014) 872–881.
[12] X. Wang, Y. Chi, T. Mu, J. Mol. Liq. 193 (2014) 262–266.
[13] M.P. Singh, R.K. Singh, S. Chandra, Prog. Mater. Sci. 64 (2014) 73–120.
[14] H. Weingärtner, Angew. Chem. Int. Ed. 47 (2008) 654–670.
[15] F. Bernardi, J.D. Scholten, G.H. Fecher, J. Dupont, J. Morais, Chem. Phys. Lett. 479 (2009) 113–116.
[16] M.-A. Neouze, J. Mater. Chem. 20 (2010) 9593–9607.
[17] E. Redel, M. Walter, R. Thomann, C. Vollmer, L. Hussein, H. Scherer, M. Krüger, C. Janiak, Chem. Eur. J. 15 (2009) 10047–10059.
[18] J. Łuczak, J. Hupka, J. Thöming, C. Jungnickel, Colloid Surf. A 329 (2008) 125–133.
[19] I. Szilagyi, T. Szabo, A. Desert, G. Trefalt, T. Oncsik, M. Borkovec, Phys. Chem. Chem. Phys. 16 (2014) 9515–9524.
[20] M.H.G. Prechtl, P.S. Campbell, J.D. Scholten, G.B. Fraser, G. Machado, C.C. Santini, J. Dupont, Y. Chauvin, Nanoscale 2 (2010) 2601–2606.
[21] M.G. Freire, C.M.S.S. Neves, I.M. Marrucho, J.A.P. Coutinho, A.M. Fernandes, J. Phys. Chem. A 114 (2010) 3744–3749.
[22] J. Łuczak, C. Jungnickel, M. Markiewicz, J. Hupka, J. Phys. Chem. B 117 (2013) 5653–5658.
[23] B. Dong, X. Zhao, L. Zheng, J. Zhang, N. Li, T. Inoue, Colloid Surf. A 317 (2008) 666–672.
[24] J. Łuczak, A. Latowska, J. Hupka Colloid Surf. A 471 (2015) 26–37.
[25] J. Łuczak, J. Hupka, J. Mol. Liq. 199 (2014) 552–558.
[26] J. Piekart, J. Luczak, Soft Matter 11 (2015) 8992–9008.
[27] P. Dash, R.W.J. Scott, Chem. Commun. 7 (2009) 812–814.
[28] J. Dupont, M.R. Meneghetti, Curr. Opin. Colloid Interface Sci. 18 (2013) 54–60.
[29] P.S. Campbell, C.C. Santini, D. Bouchu, B. Fenet, K. Philippot, B. Chaudret, A.A.H. Padua, Y. Chauvin, Phys. Chem. Chem. Phys. 12 (2010) 4217–4223.
[30] P. Migowski, D. Zanchet, G. Machado, M.A. Gelesky, S.R. Teixeira, J. Dupont, Phys. Chem. Chem. Phys. 12 (2010) 6826–6833.
[31] C.W. Scheeren, G. Machado, S.R. Teixeira, J. Morais, J.B. Domingos, J. Dupont, J. Phys. Chem. B 110 (2006) 13011–13020.
[32] M.H.G. Prechtl, M. Scariot, J.D. Scholten, G. Machado, S.R. Teixeira, J. Dupont, Inorg. Chem. 47 (2008) 8995–9001.
[33] M. Zhang, X. Xu, M. Zhang, Mater. Lett. 62 (2008) 385–388.
[34] N. Chen, K. Wang, X. Zhang, X. Chang, L. Kang, Z.-H. Liu, Colloid Surface A 387 (2011) 10–16.
[35] X. Liu, J. Ma, P. Peng, W. Zheng, Mater. Sci. Eng. B 150 (2008) 89–94.
[36] Y.-H. Lin, S. Das, C.-Y. Yang, J.-C. Sung, C.-H. Lu, J. Alloy Comp. 632 (2015) 354–360.
[37] J.-S. Xu, Y.-J. Zhu, F. Chen, Mater. Lett. 94 (2013) 104–107.
[38] L. Xu, J. Xia, H. Xu, S. Yin, K. Wang, L. Huang, L. Wang, H. Li, J. Power Sources 245 (2014) 866–874.
[39] S.-W. Cao, Y.-J. Zhu, J.-B. Cui, J. Solid State Chem. 183 (2010) 1704–1709.
[40] J. Xia, S. Yin, H. Li, H. Xu, L. Xu, Q. Zhang, Colloid Surf. A 387 (2011) 23–28.
[41] L. Jing, M. Wang, X. Li, R. Xiao, Y. Zhao, Y. Zhang, Y.-M. Yan, Q. Wu, K. Sun, Appl. Catal. B 166–167 (2015) 270–276.
[42] H. Liu, Y. Liang, H. Hu, M. Wang, Solid State Sci. 11 (2009) 1655–1660.
[43] P. Peng, X. Liu, C. Sun, J. Ma, W. Zheng, J. Solid State Chem. 182 (2009) 1003–1008.
[44] N. Yu, L. Gong, H. Song, Y. Liu, D. Yin, J. Solid State Chem. 180 (2007) 799–803.
[45] G. Nagaraju, T.N. Ravishankar, K. Manjunatha, S. Sarkar, H. Nagabhushana, R. Goncalves, J. Dupont, Mater. Lett. 109 (2013) 27–30.
[46] P. Górska, A. Zaleska, E. Kowalska, T. Klimczuk, J.W. Sobczak, E. Skwarek, W. Janusz, J. Hupka, Appl. Catal. B 84 (2008) 440–447.
[47] G. Xue, Q. Dai, S. Jiang, J. Am. Chem. Soc. 110 (1988) 2393–2395.
[48] G. Bhargava, T.A. Ramanarayanan, S.L. Bernasek, Langmuir 26 (2010) 215–219.
[49] J.M. Lázaro Martínez, E. Rodríguez-Castellón, R.M.T. Sánchez, L.R. Denaday, G.Y. Buldain, V. Campo Dall' Orto, J. Mol. Catal. A Chem. 339 (2011) 43–51.
[50] Y. Wu, H. Liu, J. Zhang, F. Chen, J. Phys. Chem. C 113 (2009) 14689–14695.
[51] A.V. Naumkin, A. Kraut-Vass, S.W. Gaarenstroom, C.J. Powell, NIST X-ray Photoelectron Spectroscopy Database 20. Version 4.1, (<http://srdata.nist.gov/xps/>), 2012.
[52] Y. Cong, J. Zhang, F. Chen, M. Anpo, J. Phys. Chem. C 111 (2007) 6976–6982.
[53] G.A. Battiston, R. Gerbasi, A. Gregori, M. Porchia, S. Cattarin, G.A. Rizzi, Thin Solid Films 371 (2000) 126–131.
[54] J. Yu, X. Zhao, Q. Zhao, Thin Solid Films 379 (2000) 7–14.
[55] E. György, A. Pérez del Pino, P. Serra, J.L. Morenza, Surf. Coat. Technol. 173 (2003) 265–270.
[56] T.H.G.N.C. Saha, J. Appl. Physiol. 72 (1992) 3072–3079.
[57] E. Grabowska, J. Reszczyńska, A. Zaleska, Water Res. 46 (2012) 5453–5471.
[58] P. Górska, A. Zaleska, J. Hupka, Sep. Purif. Technol. 68 (2009) 90–96.
[59] C. Xu, R. Killmeyer, M.L. Gray, S.U.M. Khan, Appl. Cata.l B 64 (2006) 312–317.
[60] B.K. Patricia, A. Hunt, Tom Welton, Chem. Eur. J. 12 (2006) 6762–6775.
[61] A.S. Ogunlaja, E. Hosten, Z.R. Tshentu, Ind. Eng. Chem. Res. 53 (2014) 18390–18401.